JOURNAL OF DEGRADED AND MINING LANDS MANAGEMENT
Volume 11, Number 1 (October 2023):5073-5083, doi:10.15243/jdmlm.2023.111.5073
ISSN: 2339-076X (p); 2502-2458 (e), www.jdmlm.ub.ac.id

Research Article

Mapping eruption affected area using Sentinel-2A imagery and machine learning techniques

Ni Made Trigunasih[1*], I Wayan Narka[1], Moh Saifulloh[2]

[1] Soil Sciences and Environment, Faculty of Agriculture, Udayana University, Jl. Raya Kampus UNUD, Bukit Jimbaran, Kuta Selatan, Badung-Bali 80361, Indonesia
[2] Spatial Data Infrastructure Development Center (PPIDS), Udayana University, Jl. Raya Kampus UNUD, Bukit Jimbaran, Kuta Selatan, Badung-Bali 80361, Indonesia

[*]corresponding author: trigunasih@unud.ac.id

Article history:
Received 25 May 2023
Received 1 July 2023
Accepted 1 August 2023

Keywords:
eruption
land cover
machine learning
Mount Agung-Bali
remote sensing
Sentinel-2A

Abstract

Volcanic eruptions are natural disasters with significant environmental and societal impacts. Timely detection and monitoring of volcanic eruptions are crucial for effective hazard assessment, mitigation strategies, and emergency response planning. Remote sensing technology has emerged as a valuable tool for detecting and assessing the effects of volcanic eruptions. One of the challenges in remote sensing image processing is handling large data dimensions that are difficult to address using traditional methods. Machine learning approaches offer a suitable solution to tackle these challenges. Machine learning demonstrates increasing computational capabilities, the ability to handle big data and automation. This study aimed to compare different machine learning classification algorithms, including Random Forest (RF), Support Vector Machine (SVM), Gaussian Mixture Model (GMM), and K-Nearest Neighbors (KNN). The data utilized in this study was derived from Sentinel-2A Multi-Spectral Instrument (MSI) imagery, which was tested in areas affected by the eruption of Mount Agung, Bali Province, in 2017. The results indicated that the GMM algorithm performed the best among the machine learning classifiers, achieving an Overall Accuracy (OA) value of 82.04%. It was followed by RF (78.86%) and KNN (77.55%). The areas affected by volcanic eruptions were determined by overlaying disaster-prone regions with areas mapped using the machine learning approach. The total affected area was measured as 29.89 km^2, with an additional 3.31 km^2 outside the designated zone. The findings of this study serve as a guideline for governmental entities, stakeholders, and communities to implement effective mitigation efforts for disaster risk reduction.

To cite this article: Trigunasih, N.M., Narka, I.W. and Saifulloh, M. 2023. Mapping eruption affected area using Sentinel-2A imagery and machine learning techniques. Journal of Degraded and Mining Lands Management 11(1):5073-5083, doi:10.15243/jdmlm.2023.111.5073.

Introduction

Mount eruptions are natural geological events with profound environmental implications, influencing various terrestrial and atmospheric processes. These eruptions not only result in immediate catastrophic effects, such as the release of ash, pyroclastic flows, and lava flows but also trigger long-term consequences that can significantly alter the landscape and ecological balance of affected regions (Thouret et al., 2007; Lavigne et al., 2013). The correlation between mount eruptions and land degradation, vegetation change, and the utilization of remote sensing data for monitoring and assessment has garnered increasing attention from the scientific community in recent years. Mount eruptions are known to cause extensive land degradation through mechanisms such as soil erosion, ash deposition, and alteration of landforms (Suwa and Yamakoshi, 1999; Carn et al., 2004; Komorowski et al., 2013; Harsanto, 2015).

The disturbance of natural ecosystems due to volcanic activities often leads to changes in land cover and vegetation patterns, impacting plant biodiversity, forest regeneration, and overall ecosystem resilience (Malawani et al., 2021; Saputra et al., 2022). Additionally, the socio-economic consequences of land degradation in volcanic regions can be severe, affecting local livelihoods, agriculture, and infrastructure. The impact of volcanic eruptions can be investigated using remote sensing technology approaches.

Remote sensing data obtained from various satellite and aerial platforms have proven to be valuable tools for detecting, monitoring, and analyzing volcanic eruptions and their associated impacts (Schmidt et al., 2015; Hu et al., 2022; Simurda et al., 2022). Remote sensing technology allows for the acquisition of high-resolution imagery and data over large areas, enabling the detection and monitoring of volcanic eruptions on a global scale. Satellites equipped with specialized sensors, such as multi-spectral and thermal infrared instruments, can capture the spectral signatures and thermal anomalies associated with volcanic activity. These data provide valuable information about eruption characteristics, including the size, location, duration, and intensity of volcanic events. The development of remote sensing data, from aerial photographs to digital images, cannot be separated from the history of computer development. Remote sensing data processing that requires visual interpretation with manual techniques has shifted to digital analysis techniques, so its use is growing with various techniques to improve accuracy results. The advantage of computer image analysis is that it reduces the subjective factor of human judgment. One of the problems in recognizing the spectral pattern of remote sensing data is image resolution, where the higher the resolution, the larger the data volume, and the algorithm for analysis is more complex. Thus, several algorithms were developed to be able to store large amounts of data and analyze and validate it. The knowledge-based approach then shifted to a data-based approach, which is the intersection of statistical science and computer science, namely artificial intelligence.

Artificial intelligence is widely used to solve various problems such as business, robotics, natural language, mathematics, games, perception, medical diagnosis, engineering, financial analysis, scientific analysis, and reasoning (Ruiz-Real et al., 2021). Machine learning can be defined as the application of computers and mathematical algorithms adopted utilizing learning that comes from data and produces predictions in the future (Russell and Bohannon, 2015). The learning process in question attempts to acquire intelligence through training and testing (Blum, 2007; Bensoussan et al., 2022). The field of machine learning is concerned with how to build computer programs to improve automatically based on experience. Recent research reveals that machine learning is divided into three categories: supervised learning, unsupervised learning, and reinforcement learning (Huang et al., 2006). The technique used by supervised learning is a classification method in which the data set is completely labeled to classify the unknown class. At the same time, the unsupervised learning technique is often called a cluster because there is no need for labeling in the data set, and the results do not identify examples in the specified class (Thupae et al., 2018; Favorskaya et al., 2021).

The supervised learning method is based on a collection of data samples with labels. The sample set is used to summarise the characteristics of the behavior size distribution in each type of application to form a behavioral model from the data (Wu et al., 2011). Supervised learning has several popular algorithms, such as Back Propagation (BP), Linear Regression (LR), Random Forest (RF), Naive Bayesian (NB), Rocchio Method (RM), Decision Tree (DF), and Neural Network (NN) (Negnevitsky et al., 2005; Negnevitsky and Pavlovsky, 2005; Portugal et al., 2018; Uddin et al., 2019; Batta, 2020). Then, several algorithms for classification are also mentioned, such as Support Vector Machines (SVM), Normal Bayesian Classifier (NBC), K-Nearest Neighbors (KNN), Gradient Boosted Trees (GBT), Random Trees (RT), and Artificial Neural Networks (ANN), Gaussian Mixture Models (GMM) (Wang Z et al., 2020; Ravichandran et al., 2021). The use of machine learning algorithms in remote sensing has been carried out for the detection of land use changes, landslide susceptibility, flood susceptibility, and detection of certain types of plants on agricultural land (Prins and Van Niekerk, 2020; Talukdar et al., 2020; Hashi et al., 2021; Ma et al., 2021).

The object of this research is the disaster-prone area (KRB) of the eruption of Mount Agung. The enormous eruption of Mount Agung occurred in 1963. At the beginning of the 21st century, in 2017, it erupted again, which caused losses for the tourism sector in Bali. The use of multi-spectral satellite imagery data on Sentinel 2 images and a combination of machine learning and remote sensing technology can detect the spatial distribution of land that lava flows have excavated due to the eruption.

The purpose of this study was to compare machine learning algorithms on remote sensing imagery. The second goal was to combine these algorithms to detect the spatial distribution of the impact of lava flows due to the 2017 eruption.

Methods

The research employed a descriptive qualitative approach to investigate the impacts of volcanic eruptions derived from remote sensing data. Data analysis for remote sensing images using automated supervised machine learning methods, namely the KNN, RF, and GMM. RF is a supervised machine learning algorithm that is often used in classification

and regression problems. RF is also called the ensemble method, which is a method to improve classification accuracy by combining classification methods (Sheykhmousa et al., 2020). GMM is a probabilistic model and uses a soft clustering approach to distribute points in different clusters. This GMM has a Gaussian distribution with a bell-shaped curve, with data points distributed symmetrically around the mean (Wang Z et al., 2020). KNN is a non-parametric algorithm that does not make any assumptions about the data. KNN is a machine learning algorithm with a supervised learning approach that works by classifying new data using the similarity between new data and several data (k) at the closest available location. This algorithm implements 'lazy learning" or "instant-based learning" and is a non-parametric algorithm. KNN algorithm is used for classification and regression (Brownlee, 2016).

Research site

Spatially, the research was carried out in the disaster-prone area of Mount Agung with centroid coordinates 8°20'37.60"S, 115°30'27.04"E (Figure 1). The area of the research object for detecting land use and lava flows is 33.20 km^2. The disaster-prone area is located in Karangasem Regency, with an area ranging from 600 to 3000 m above sea level. Administratively, 21 villages are included in the disaster-prone area. Among them are the villages of Besakih, Sebudi, Ban, Sukadana, Tulamben, Jungutan, Dukuh, Budakeling, etc. The slope level of the areas ranges from flat (0-8%) to very steep (>45%).

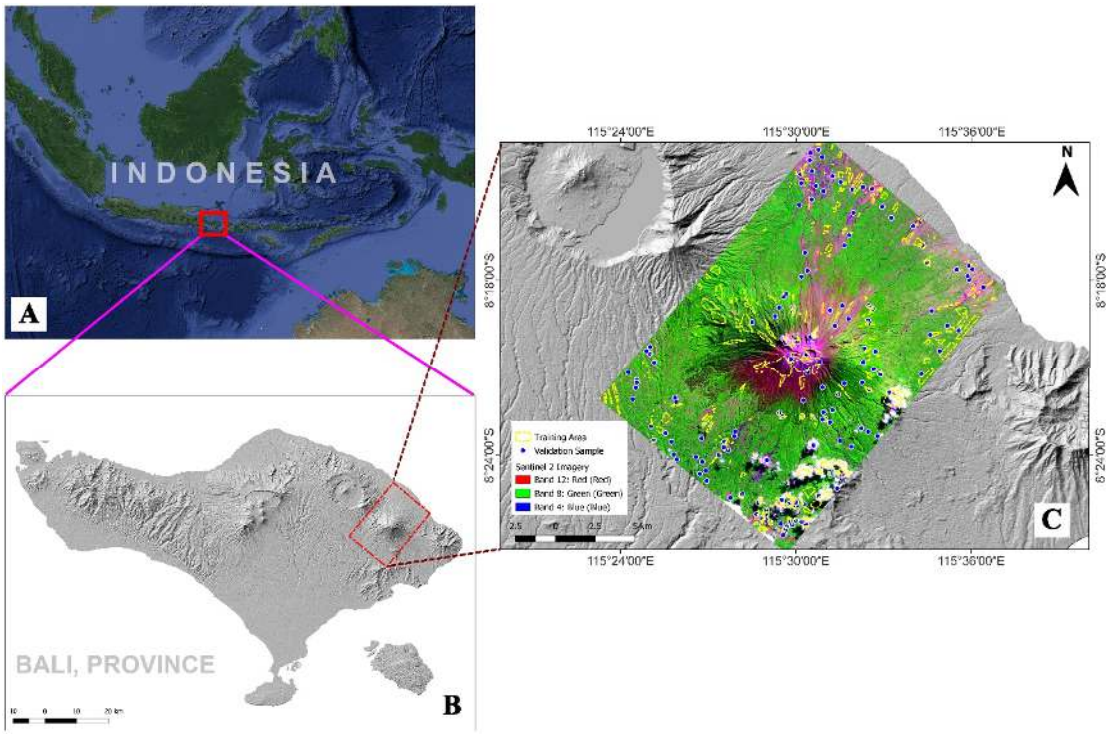

Figure 1. The research location is viewed from a global (a), regional (b) scale, as well as a combination of false colors to facilitate training and validation/testing of data on a local scale (c).

Tools and materials

This study used a single image acquisition in May 2018 on Citra Sentinel-2 Level 1 C (https://scihub.copernicus.eu/dhus/#/home). The Sentinel-2A Satellite with Multi-Spectral Instrument (MSI) has 13 spectral channels. It extends from Visible and Near Infrared (VNIR). It displays four spectral channels with a spatial resolution of 10 m, namely blue (490 nm), green (560 nm), red (665 nm), and near-infrared (842 nm) channels. Short Wave Infrared (SWIR) displays six channels with a spatial resolution of 20 m, namely four channels in spectral vegetation (705 nm, 740 nm, and 865 nm) and two large SWIR channels (1,610 nm and 2,190 nm). Three channels with a spatial resolution of 60 m were used for atmospheric correction and cloud screening (443 nm for aerosol capture, 945 nm for water vapor capture, and 1,380 nm for cirrus cloud detection). This satellite has a swept area of 290 km (Bergsma and Almar, 2020; Phiri et al., 2020). Village administrative boundaries were obtained from the Ministry of Agrarian and Spatial Planning in 2019, while disaster-prone areas (KRB) were obtained from PVMBG (https://vsi.esdm.go.id). The data processing was carried out using QGIS software and the additional *dzetsaka* plugin, and validation was done using the Semi-Automatic Classification Plugin (SCP).

Research method

The Sentinel-2 image used is level 1C 2018 data that had been geometrically and radiometrically corrected. The pre-processing stage of the Sentinel-2 image was carried out on QGIS software version 3.22 using the Semi-Automatic Classification Plugin, which included atmospheric correction, resampling, and image cropping. Atmospheric correction was carried out using the Dark Object Subtraction (DOS) method to reduce atmospheric disturbances and make recognizing an object or other appearance easier. The next step was to combine 13 bands of the corrected image in one image. The number of samples was 500 polygons, which represented the land cover of dense vegetation, sparse vegetation, agriculture, bare land, settlement, and cloud cover. Of the 500 samples, 350 (70%) were used as training, and 150 (30%) were used as testing/validation. The spatial distribution of the training area and testing/validation are presented in Figure 1c. The output of the validation is the accuracy of the land cover classification of each machine learning method. The accuracy test aims to evaluate the error rate in the classification results to determine the percentage accuracy of the classification results. The accuracy test was performed on the classified image without delineation. Accuracy is calculated by an error matrix (confusion matrix). The percentage of the results of each image composition is seen from the producer accuracy, user accuracy, overall accuracy, and kappa accuracy.

Results and Discussion

Signature reflectance in different land cover types

The spectral signature is generated using the bands presented by Sentinel Image 2. It is defined as a characteristic response pattern as each object on the earth's surface has its interaction with electromagnetic energy. The basis of the classification is to find some areas of the electromagnetic spectrum where the nature of this interaction differs for each object or land cover on the earth's surface (Wang B et al., 2018; Salih, 2021). Understanding the spectral signatures of different objects and features is essential for accurate classification and mapping in remote sensing applications. Sentinel-2A's multi-spectral sensor, with its 13 spectral bands, provides rich information to differentiate various land cover and land use categories. By analyzing the spectral response of objects and applying appropriate classification algorithms, researchers and analysts can derive valuable insights about the earth's surface, monitor changes over time, and support a wide range of applications, including environmental monitoring, agriculture, urban planning, and natural resource management.

The classification algorithm uses the spectral signature, which makes it possible to label image pixels. Different types of land cover have different spectral values (vegetation, bare land, built-up land). In Figure 2, it can be seen that each material has a unique signature. Therefore, this spectral signature can be used for the classification of materials such as land cover, vegetation, water, and asphalt/construction, depending on the sensor resolution and the amount and type of land cover that can be identified. The amount of reflected radiation concerning the wavelength is observed, in which the response of the spectral signature increases to infrared. Regarding vegetation, it is a resource that depends on many characteristics depending on the type of species to be evaluated (leaves, stems, stems, moisture, etc.) (Borgogno-Mondino et al., 2020; Kobayashi et al., 2020). The reflectance increases in the near-infrared due to plants' low energy absorption.

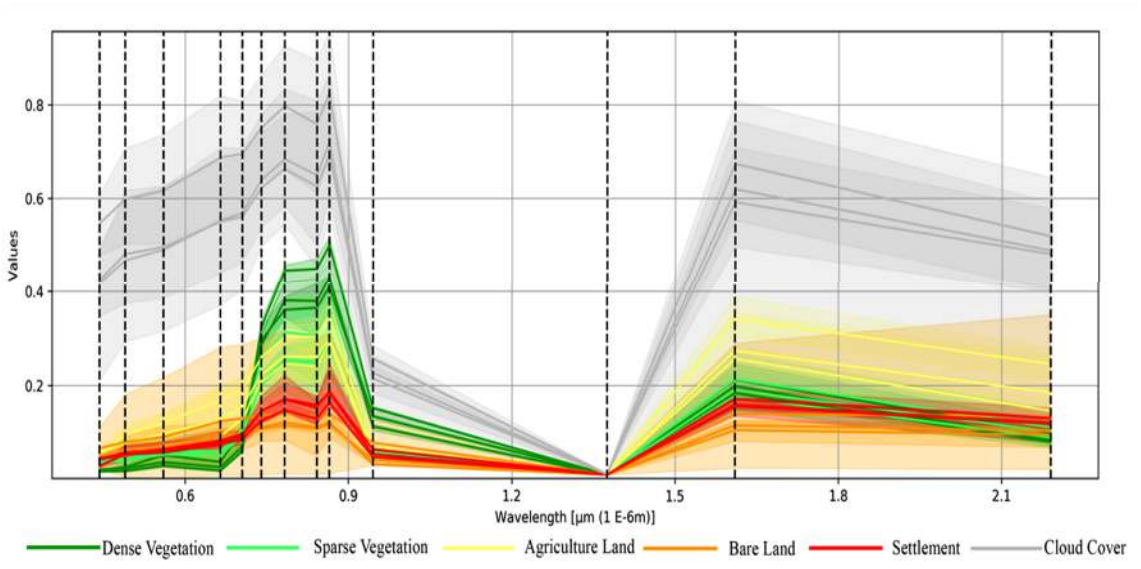

Figure 2. Signature reflectance in different land cover types.

In the mid-infrared, there is a significant decrease along the wavelength, as water in plants absorbs energy. The spectral behavior depends on several characteristics, such as air and water content, structure, and texture. In this case, when dealing with construction enclosures such as buildings and vacant lots, they are smooth surfaces, implying that the reflectance increases along the wavelength. Sequentially, the lowest reflectance value was found in the land cover of bare land, settlement, agriculture, sparse vegetation, and dense vegetation, and the highest reflectance value was cloud cover.

Spatial distribution of land cover types

The results of land cover classification using machine learning algorithms KNN, RF, and GMM are presented in Figure 3. The classification of cover in this study consists of dense vegetation, sparse vegetation, agricultural land, bare land used by lahars/eruption impacts, settlements, and cloud cover. Dense vegetation includes forest land use, as well as shrubs with a high density. Sparse vegetation is included in the use of scrubland with low gaps between trees and fields.

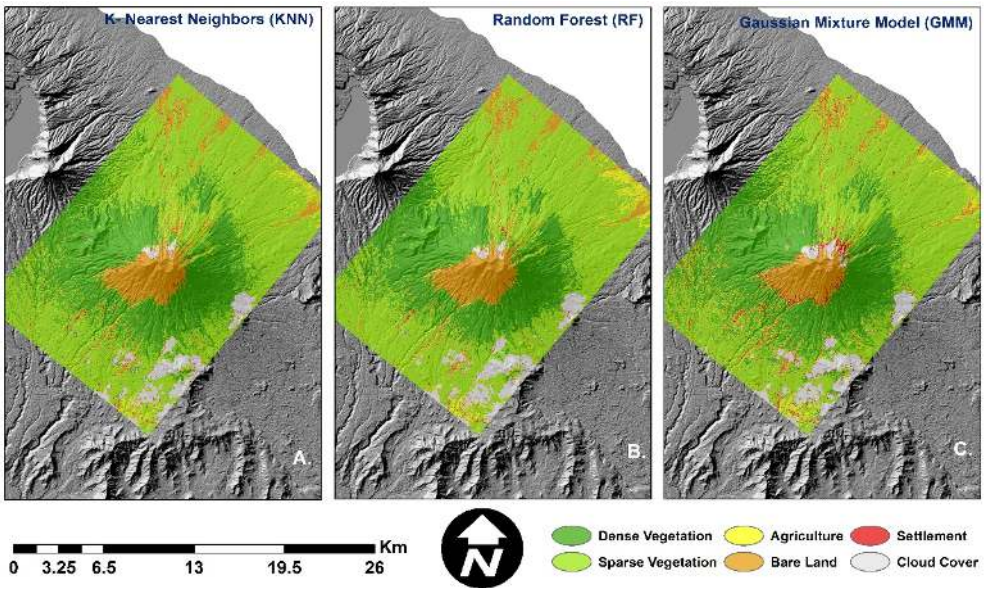

Figure 3. Comparison of land cover classification of machine learning KNN (a), RF (b), and GMM (c).

Agricultural land includes the use of paddy fields. The bare land indicates the former lava flows from the eruption, such as a heap of sand. Settlements include using construction land, buildings, road networks and partly using bare land. Visually, the KNN and RF algorithms have the same pattern. Unlike the case with the GMM algorithm, because it appears on the upper slopes of Mount Agung, there are settlements in the red area. The sparse vegetation has the most expansive area in all machine learning algorithms. This is followed by dense vegetation, bare land, cloud cover, agriculture, and settlements. A very contrasting area difference is shown in the cover of settlement land and bare land. The bare land of the KNN and RF algorithms has an area of 29 km^2, while the GMM algorithm has an area of only 22 km^2. The settlement of the KNN and RF algorithms is 4 km^2, while the GMM algorithm is 12 km^2 (Figure 4).

Accuracy assessment in differential machine learning algorithm

Based on machine learning classification on remote sensing imagery, the highest accuracy was found in the use of the GMM algorithm with OA (82.04) and Kappa (0.74), followed by the RF algorithm with OA (78.86) and Kappa (0.70), and the lowest accuracy was the KNN algorithm with OA (77.55) and Kappa (0.69) (Table 1). Based on the classification results, RF has a pattern closer to the training data results on the original image, although it has lower accuracy than the GMM classification results. This is because the parametric classification is strongly influenced by the distribution of pixels evenly in each pattern and can only better recognize patterns with the same tendency for pixel values as the sample data. At the same time, non-parametric can understand the data even though it has noise (interference). Classification accuracy is also influenced by the user's accuracy in determining the sample area; a more detailed classification scheme and field testing are needed (Tavares et al., 2019; Jamali, 2021; Loukika et al., 2021; Shetty et al., 2021). In Figure 5, the bare land is detected as a settlement, and the most significant error is shown by the pattern of the GMM classification results. RF offers advantages over KNN and GMM, which are more consistent and do not get stuck in local minimums. There is no need to repeat the training by trial and error on each parameter or random initialization.

Table 1. Accuracy assessment of land use/ land cover (LULC) based on machine learning method.

LULC	Standard Error (SE)			Producer's Accuracy (PA) %			User's Accuracy (UA) %			Overall Accuracy (OA) %			Kappa		
	KNN	RF	GMM	KNN	RF	GMM	KNN	RF	GMM	KNN	RF	GMM	KNN	RF	GMM
DV	0.00	0.009	0.01	100.00	100.00	100.00	100.00	96.77	96.77	77.55	78.86	82.04	0.69	0.70	0.74
SV	0.040	0.042	0.04	100.00	100.00	97.05	59.52	65.79	70.59						
AL	0.026	0.020	0.03	21.27	40.85	24.63	100.00	100.00	93.33						
BL	0.022	0.023	0.02	64.13	63.14	55.83	91.18	93.94	90.32						
ST	0.033	0.038	0.03	7.16	6.82	28.58	64.29	78.57	65.22						
CC	0.003	0.005	0.00	100.00	100.00	100.00	93.75	83.33	93.75						

Where: Dense Vegetation (DV), Sparse Vegetation (SV), Agricultural Land (AL), Bare Land (BL), Settlement (ST), and Cloud Cover (CV).

Machine learning algorithms: K-Nearest Neighbors (KNN), Random Forest (RF), Gaussian Mixture Model (GMM).

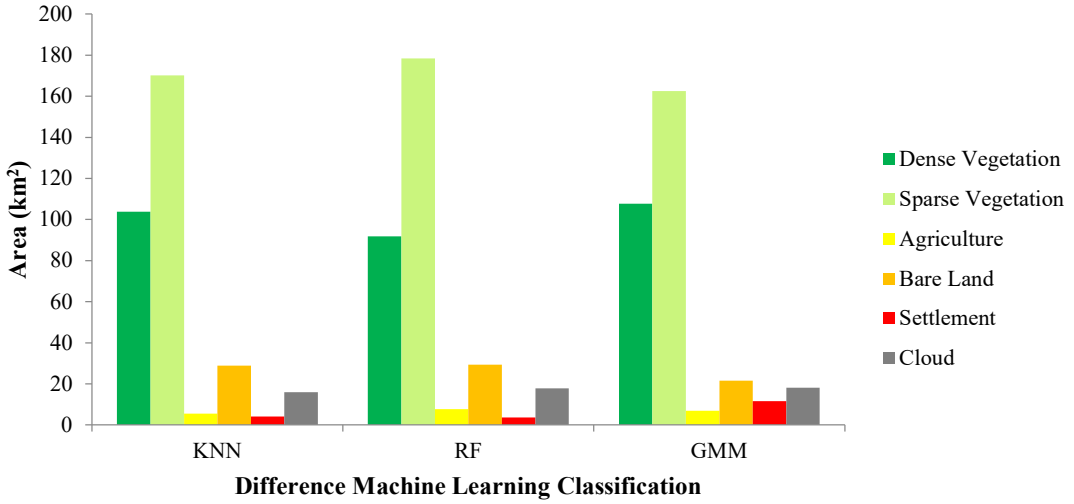

Figure 4. Graph of the area of each land cover type.

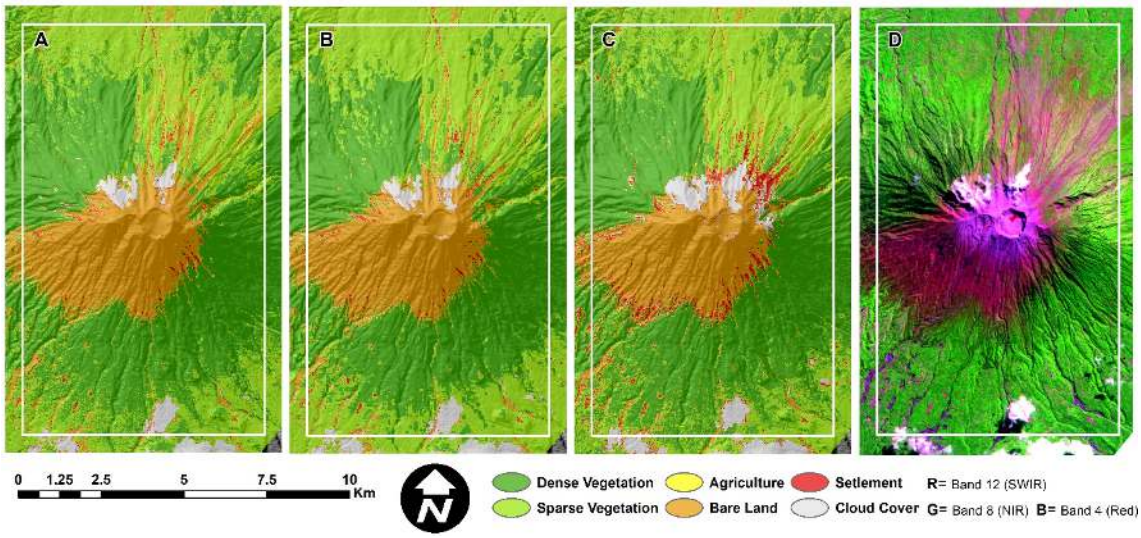

Figure 5. Comparison of the original image (d) with the prediction results on the KNN (a), RF (b), and GMM algorithms (c).

Eruption affected area

The area affected by the eruption was obtained by combining vacant land in the KNN, RF, and GMM algorithms with the aim of obtaining a representative coverage of the affected area based on satellite imagery used by researchers. The area affected by the eruption is spatially indicated by the black zone. Spatially, the widest eruption impact is located in the northwest, north, and northeast, and there are some areas in the south. The eruption scars are shown to follow river patterns, so most of them are deposited in the northern coastal area (Figure 6). Based on the disaster-prone zone (KRB), the eruption impact is included in KRB III (21.11 km^2), KRB II (8.14 km^2), KRB I (0.53 km^2), and outside KRB (3.31 km^2) presented by Figure 7. The widest spatial distribution of the eruption impact is in Sebudi Village (7.17 km^2), Besakih (6.14 km^2), Ban (4.36 km^2), Sukadana (4.27 km^2), Tianyar (2.91 km^2), and several other areas around Mount Agung disaster prone area (Figure 8). The eruption had a detrimental impact on agricultural land use and the tourism sector (Rahmawati et al., 2019). Previous researchers have mapped vegetation changes near Mount Agung using a vegetation index approach on Landsat images. Their findings indicate an increase (approximately 1 km^2) in vegetation cover from the 1980s to 2016. The vegetation change near the crater of Mount Agung is relatively slow compared to other volcanoes, such as Mount Merapi (Sutomo and Wahab, 2019). Recent researchers have reported that the artificial neural network (ANN) machine learning algorithm is more accurate than the support vector machine (SVM), with accuracies of 94.67% and 97%, respectively (Syifa et al., 2020).

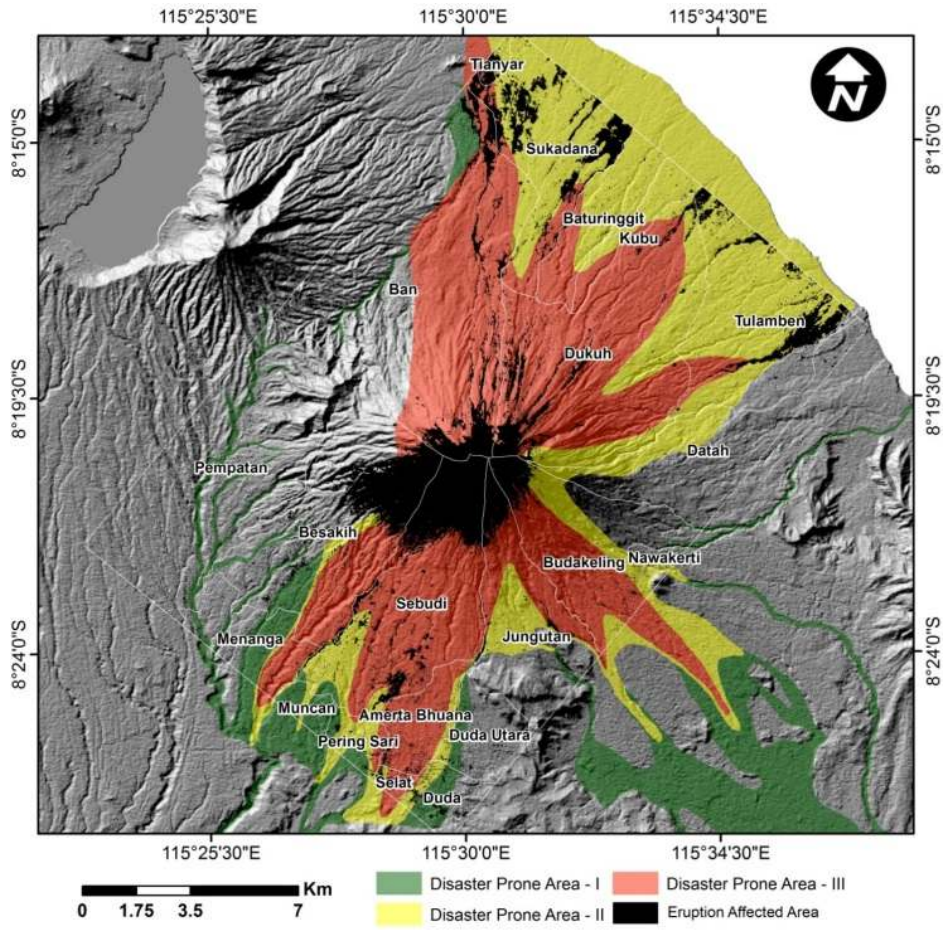

Figure 6. Spatial distribution of eruption-affected areas with a base map of disaster-prone areas (KRB).

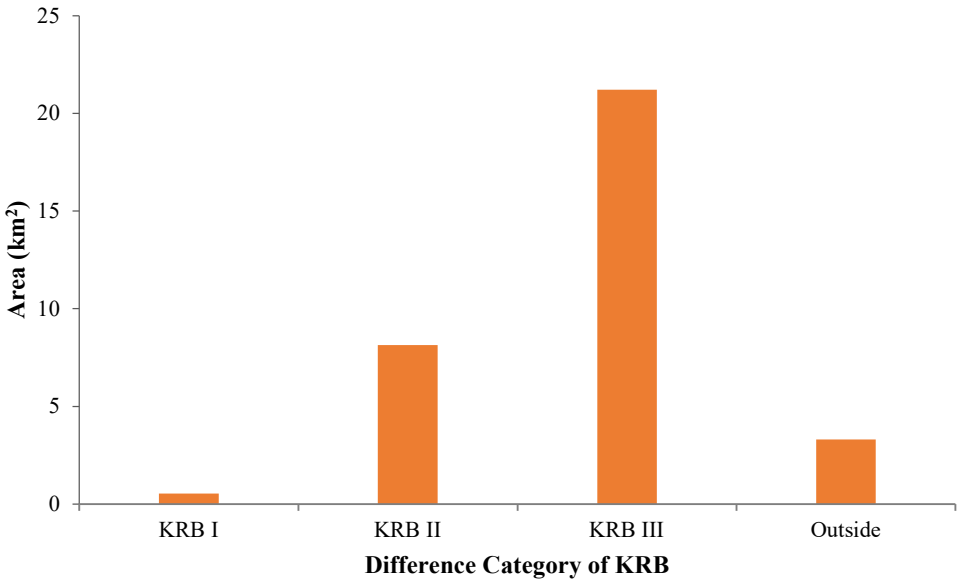

Figure 7. The difference in the area affected in each KRB category.

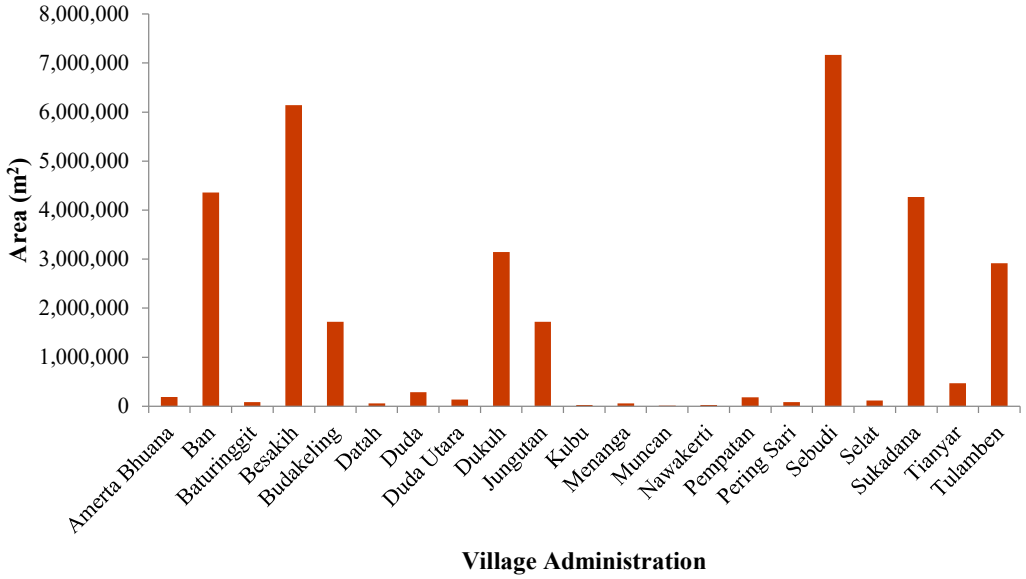

Figure 8. Eruption affected area.

The previous researchers used Landsat imagery with a relatively low spatial resolution (30 m/pixel) and a relatively high cloud cover. The drawback was that the images did not detect affected areas with dimensions less than 30 m/pixel and areas obscured by clouds. The Sentinel-2A imagery used in this study has a higher spatial resolution of 10 m/pixel and less than 10% cloud cover, ensuring that the entire eruption-affected area is captured in the images used for this study. The spatial distribution of the affected areas is relatively accurate, following the pattern of river flow from upstream to downstream (Figure 6).

More detailed mapping results have been investigated by Andaru et al. (2021), who reconstructed the lava dome using Digital Terrain Model (DTM) data obtained from unmanned aerial vehicles. The difference between the 2017 and 2019 DTMs revealed a total erupted material volume (886,100 ± 8,000 m^3) deposited on the surrounding slopes. Optical sensor image products (such as Landsat and Sentinel-2A) cannot reconstruct such models. Integrating high-resolution, temporal, and spectral remote sensing data with active-passive sensor systems can be used to estimate more accurate models. Image classification techniques with appropriate algorithms and a relatively large number of training samples can approximate field conditions. The integration of remote sensing data and machine learning techniques offers a powerful approach to mapping volcanic eruption effects. By harnessing the capabilities of Sentinel-2A and the computational power of machine learning algorithms, we could accurately identify and map the areas impacted by volcanic activities. This information is crucial for assessing the extent of damage, understanding the distribution of hazards, and guiding mitigation efforts. Future studies could explore the incorporation of additional data sources, such as thermal imagery or Synthetic Aperture Radar (SAR), to further enhance the detection and characterization of eruption effects. Additionally, the integration of multi-temporal datasets could provide valuable insights into the dynamic nature of volcanic activities and their long-term impacts on the environment.

Sentinel-2A imagery and machine learning algorithms effectiveness in mapping volcanic eruption effects. The high-resolution imagery and accurate classification results enable a detailed assessment of the affected areas and facilitate information for disaster management and mitigation. The integration of remote sensing and machine learning techniques holds great potential for advancing our understanding of volcanic eruptions and their environmental impacts.

Conclusions

Remote sensing data can describe the phenomenon of the eruption impact and other land covers around Mount Agung. The dynamics on the earth's surface can be detected by combining remote sensing and machine learning. Land cover detected by machine learning includes dense vegetation, sparse vegetation, agricultural land, bare land or former lahars, settlements, and cloud cover. The best machine learning algorithm in this study is the Gaussian Mixture Model (GMM) with an OA value of 82.04, followed by Random Forest (RF) (78.86%) and K-Nearest Neighbors (KNN) (77.55%). Visually, the RF algorithm has a spatial pattern similar to the original image on Sentinel-2A. So, it is necessary to do further research on multi-spectral images with more training and testing data to get a consistent pattern for each of these algorithms. The areas affected by volcanic

eruptions were determined by overlaying disaster-prone regions with areas mapped using the machine learning approach. The total affected area was measured as 29.89 km^2, with an additional 3.31 km^2 outside the designated zone. The findings of this study can be used as a guideline for the government, stakeholders, and the community to carry out mitigation efforts for disaster risk reduction (DRR).

Acknowledgment

The authors thank the Institute for Research and Community Service (LPPM) of Udayana University for providing the 2022 PNPB research grant.

References

Andaru, R., Rau, J.Y., Syahbana, D.K., Prayoga, A.S. and Purnamasari, H.D. 2021. The use of UAV remote sensing for observing lava dome emplacement and areas of potential lahar hazards: An example from the 2017–2019 eruption crisis at Mount Agung in Bali. *Journal of Volcanology and Geothermal Research* 415, doi:10.1016/j.jvolgeores.2021.107255

Batta, M. 2020. Machine learning algorithms - a review. *International Journal of Science and Research* 9(1):381-386, doi:10.21275/ART20203995.

Bensoussan, A., Li, Y., Nguyen, D.P.C., Tran, M.B., Yam, S.C.P. and Zhou, X. 2022. Machine learning and control theory. *Handbook of Numerical Analysis* 23, doi:10.1016/bs.hna.2021.12.016.

Bergsma, E.W.J. and Almar, R. 2020. Coastal coverage of ESA' Sentinel 2 mission. *Advances in Space Research* 6511, doi:10.1016/j.asr.2020.03.001.

Blum, A. 2007. *Machine Learning Theory*. Carnegie Melon University, School of Computer Science.

Borgogno-Mondino, E., De Palma, L. and Novello, V. 2020. Investigating Sentinel 2 multi-spectral imagery efficiency in describing the spectral response of vineyards covered with plastic sheets. *Agronomy* 1012, doi:10.3390/agronomy10121909.

Brownlee, J. 2016. K-Nearest Neighbors for Machine Learning. In: Machine Learning Algorithms, Machine Learning Mastery, /.

Carn, S.A., Watts, R.B., Thompson, G. and Norton, G.E. 2004. Anatomy of a lava dome collapse: The 20 March 2000 event at Soufrière Hills Volcano, Montserrat. *Journal of Volcanology and Geothermal Research* 131(3-4):241-264, doi: 10.1016/S0377-0273(03)0364-0.

Favorskaya, M.N., Favorskaya, A.V., Petrov, I.B. and Jain, L.C. 2021. Recent advances in numerical methods, machine learning, and computer science. In Smart Innovation, Systems and Technologies 215, doi:10.1007/978-981-33-4619-2_1.

Harsanto, P. 2015. River morphology modeling at the downstream of Progo River post-eruption 2010 of Mount Merapi. *Procedia Environmental Sciences* 28, doi:10.1016/j.proenv.2015.07.021.

Hashi, A.O., Abdirahman, A.A., Elmi, M.A., Hashi, S.Z.M. and Rodriguez, O.E.R. 2021. A real-time flood detection system based on machine learning algorithms with an emphasis on deep learning. *International Journal of Engineering Trends and Technology* 69(5):249-256, doi:10.14445/22315381/IJETT-V69I5P232.

Hu, Y., Li, Z., Wang, L., Chen, B., Zhu, W., Zhang, S., Du, J., Zhang, X., Yang, J., Zhou, M., Liu, Z., Wang, S., Miao, C., Zhang, L. and Peng, J. 2022. Rapid interpretation and analysis of the 2022 eruption of Hunga Tonga-Hunga Hàapai volcano with integrated remote sensing techniques. *Geomatics and Information Science of Wuhan University* 472, doi:10.13203/j.whugis20220050.

Huang, G.B., Zhu, Q.Y. and Siew, C.K. 2006. Extreme learning machine: Theory and applications. *Neurocomputing* 70(1-3):489-501, doi:10.1016/j.neucom.2005.12.126.

Jamali, A. 2021. Land use land cover mapping using advanced machine learning classifiers. *Ekologia (Bratislava)* 40(3):286-300, doi:10.2478/eko-2021-0031.

Kobayashi, N., Tani, H., Wang, X. and Sonobe, R. 2020. Crop classification using spectral indices derived from Sentinel-2A imagery. *Journal of Information and Telecommunication* 4(1):67-90, doi:10.1080/24751839.2019.1694765.

Komorowski, J.C., Jenkins, S., Baxter, P.J., Picquout, A., Lavigne, F., Charbonnier, S., Gertisser, R., Preece, K., Cholik, N., Budi-Santoso, A. and Surono. 2013. Paroxysmal dome explosion during the Merapi 2010 eruption: Processes and facies relationships of associated high-energy pyroclastic density currents. *Journal of Volcanology and Geothermal Research* 261:260-294, doi:10.1016/j.jvolgeores.2013.01.007.

Lavigne, F., Degeai, J.P., Komorowski, J.C., Guillet, S., Robert, V., Lahitte, P., Oppenheimer, C., Stoffel, M., Vidal, C.M., Suronoh, Pratomo, I., Wassmer, P., Hajdas, I., Hadmoko, D.S. and De Belizal, E. 2013. Source of the great A.D. 1257 mystery eruption unveiled Samalas volcano, Rinjani Volcanic Complex, Indonesia. *Proceedings of the National Academy of Sciences of the United States of America* 110(42):16742-16747, doi:10.1073/pnas.1307520110.

Loukika, K.N., Keesara, V.R., and Sridhar, V. 2021. Analysis of land use and land cover using machine learning algorithms on Google Earth engine for Munneru river basin, India. *Sustainability (Switzerland)* 13(24):13758, doi:10.3390/su132413758.

Ma, Z., Mei, G. and Piccialli, F. 2021. Machine learning for landslides prevention: a survey. *Neural Computing and Applications* 33(17):10881-10907, doi:10.1007/s00521-020-05529-8.

Malawani, M.N., Lavigne, F., Gomez, C., Mutaqin, B.W. and Hadmoko, D.S. 2021. Review of local and global impacts of volcanic eruptions and disaster management practices: The Indonesian example. *Geosciences (Switzerland)* 11(3):109, doi:10.3390/geosciences11030109.

Negnevitsky, M. and Pavlovsky, V. 2005. Neural networks approach to online identification of multiple failures of protection systems. *IEEE Transactions on Power Delivery* 20(2):588-594, doi:10.1109/TPWRD.2004.843451.

Negnevitsky, M., Lim, M.J.H., Hartnett, J. and Reznik, L. 2005. Email communications analysis: How to use computational intelligence methods and tools? *Proceedings of the 2005 IEEE International Conference on Computational Intelligence for Homeland Security and Personal Safety*, CIHSPS 2005, doi:10.1109/CIHSPS.2005.1500603.

Phiri, D., Simwanda, M., Salekin, S., Nyirenda, V.R., Murayama, Y. and Ranagalage, M. 2020. Sentinel-2 data

for land cover/use mapping: A review. *Remote Sensing* 12(14):2291, doi:10.3390/rs12142291.

Portugal, I., Alencar, P. and Cowan, D. 2018. The use of machine learning algorithms in recommender systems: A systematic review. *Expert Systems with Applications* 97(1):205-227, doi:10.1016/j.eswa.2017.12.020

Prins, A.J. and Van Niekerk, A. 2020. Crop type mapping using LiDAR, Sentinel-2 and aerial imagery with machine learning algorithms. *Geo-spatial Information Science* 24(2):211-227, doi:10.1080/10095020.2020.1782776.

Rahmawati, P.I., Trianasari, N. and Martin, A.A.N.Y. 2019. The Economic Impact of Mount Agung Eruption on Bali Tourism. *Proceedings of the International Conference on Tourism, Economics, Accounting, Management, and Social Science,* doi:10.2991/teams-18.2019.18.

Ravichandran, T., Gavahi, K., Ponnambalam, K., Burtea, V. and Mousavi, J.S. 2021. Ensemble-based machine learning approach for improved leak detection in water mains. *Journal of Hydroinformatics* 23(2):307-323, doi:10.2166/HYDRO.2021.093.

Ruiz-Real, J.L., Uribe-Toril, J., Torres, J.A. and Pablo, J.D.E. 2021. Artificial intelligence in business and economics research: Trends and future. *Journal of Business Economics and Management* 22(1):98-117, doi:10.3846/jbem.2020.13641.

Russell, S. and Bohannon, J. 2015. Artificial intelligence. Fears of an AI pioneer. Science New York.

Salih, M.M. 2021. Developing spectral reflectance measurement system for environmental remote sensing applications. *International Journal of Design and Nature and Ecodynamics* 16(1):33-39, doi:10.18280/ijdne.160105.

Saputra, D.D., Sari, R.R., Hairiah, K., Widianto, Suprayogo, D. and van Noordwijk, M. 2022. Recovery after volcanic ash deposition: vegetation effects on soil organic carbon, soil structure and infiltration rates. *Plant and Soil* 474(1-2):163-179, doi:10.1007/s11104-022-05322-7.

Schmidt, A., Leadbetter, S., Theys, N., Carboni, E., Witham, C.S., Stevenson, J.A., Birch, C.E., Thordarson, T., Turnock, S., Barsotti, S., Delaney, L., Feng, W., Grainger, R.G., Hort, M.C., Höskuldsson, Á., Ialongo, I., Ilyinskaya, E., Jóhannsson, T., Kenny, P., … Shepherd, J. 2015. Satellite detection, long-range transport, and air quality impacts of volcanic sulfur dioxide from the 2014-2015 flood lava eruption at Bárðarbunga (Iceland). *Journal of Geophysical Research* 120(18), doi:10.1002/2015JD023638.

Shetty, S., Gupta, P.K., Belgiu, M. and Srivastav, S.K. 2021. Assessing the effect of training sampling design on the performance of machine learning classifiers for land cover mapping using multi-temporal remote sensing data and Google Earth engine. *Remote Sensing* 13(8):1433, doi:10.3390/rs13081433.

Sheykhmousa, M., Mahdianpari, M., Ghanbari, H., Mohammadimanesh, F., Ghamisi, P. and Homayouni, S. 2020. Support vector machine versus random forest for remote sensing image classification: a meta-analysis and systematic review. *IEEE Journal of Selected Topics in Applied Earth Observations and Remote Sensing* 13:6308-6322, doi:10.1109/JSTARS.2020.3026724.

Simurda, C., Magruder, L.A., Markel, J., Garvin, J.B. and Slayback, D.A. 2022. ICESat-2 Applications for Investigating Emerging Volcanoes. *Geosciences (Switzerland)* 12(1):40, doi:10.3390/geosciences12010040.

Sutomo, and Wahab, L. 2019. Changes in vegetation on Mount Agung Volcano Bali, Indonesia. *Journal of Tropical Biodiversity and Biotechnology* 4(2):54-61, doi:10.22146/jtbb.41008.

Suwa, H. and Yamakoshi, T. 1999. Sediment discharge by storm runoff at volcanic torrents affected by eruption. *Zeitschrift Fur Geomorphologie, Supplementband* 114.

Syifa, M., Kadavi, P.R., Lee, C.W. and Pradhan, B. 2020. Landsat images and artificial intelligence techniques used to map volcanic ashfall and pyroclastic material following the eruption of Mount Agung, Indonesia. *Arabian Journal of Geosciences* 133:1-12, doi:10.1007/s12517-020-5060-2.

Talukdar, S., Singha, P., Mahato, S., Shahfahad, Pal, S., Liou, Y.A. and Rahman, A. 2020. Land-use land-cover classification by machine learning classifiers for satellite observations-A review. *Remote Sensing* 12(7):1135, doi:10.3390/rs12071135.

Tavares, P.A., Beltrão, N.E.S., Guimarães, U.S. and Teodoro, A.C. 2019. Integration of sentinel-1 and sentinel-2 for classification and LULC mapping in the urban area of Belém, eastern Brazilian Amazon. *Sensors (Switzerland)* 19(5):1140, doi:10.3390/s19051140.

Thouret, J.C., Lavigne, F., Suwa, H., Sukatja, B. and Surono. 2007. Volcanic hazards at Mount Semeru, East Java (Indonesia), with emphasis on lahars. *Bulletin of Volcanology* 70:221-244, doi:10.1007/s00445-007-0133-6.

Thupae, R., Isong, B., Gasela, N. and Abu-Mahfouz, A.M. 2018. Machine learning techniques for traffic identification and classification in SDWSN: A survey. *Proceedings: IECON 2018 - 44th Annual Conference of the IEEE Industrial Electronics Society*, doi:10.1109/IECON.2018.8591178.

Uddin, S., Khan, A., Hossain, M.E. and Moni, M.A. 2019. Comparing different supervised machine learning algorithms for disease prediction. *BMC Medical Informatics and Decision Making* 19(1):281, doi:10.1186/s12911-019-1004-8.

Wang, B., Jia, K., Liang, S., Xie, X., Wei, X., Zhao, X., Yao, Y. and Zhang, X. 2018). Assessment of Sentinel-2 MSI spectral band reflectances for estimating fractional vegetation cover. *Remote Sensing* 10(12):1927, doi:10.3390/rs10121927.

Wang, Z., Ritou, M., Da Cunha, C., and Furet, B. 2020. Contextual classification for smart machining based on unsupervised machine learning by Gaussian mixture model. *International Journal of Computer Integrated Manufacturing* 33(10-11):1042-1054, doi:10.1080/0951192X.2020.1775302.

Wu, A., Dong, H., Wu, Q. and Ling, L. 2011. A survey of application-level protocol identification based on machine learning. *Proceedings - 2011 4th International Conference on Information Management, Innovation Management and Industrial Engineering, ICIII 2011*, 3, doi:10.1109/ICIII.2011.331.